JETIR.ORG ISSN: 2349-5162 | ESTD Year : 2014 | Monthly Issue
JOURNAL OF EMERGING TECHNOLOGIES AND INNOVATIVE RESEARCH (JETIR)
An International Scholarly Open Access, Peer-reviewed, Refereed Journal

Synthesis, Characterization, and Biomedical Applications of Transition Metal (Mn, Zn, Cu) Schiff Base Complexes: A Multifunctional Material for Healthcare and Industrial Applications

Authors

Anshu Shrivastava[1]*, Dr. P.K. Sharma[2], Dr. A. Mishra.

[1]Research Scholar, School of Physics, DAVV, Indore (M.P.), India

[2]Professor, Govt. Holkar Science College, Indore(M.P.), India
*Corresponding Author: anshuushrivastava@yahoo.com

Abstract

Schiff base coordination complexes represent a versatile class of materials with exceptional therapeutic and industrial potential. This study synthesizes and comprehensively characterizes 12 bis(N-alkyl-1-(pyridin-2-yl)methanimine) metal(II) chloride complexes incorporating Mn(II), Zn(II), and Cu(II) metals with four alkyl chain variants (L1–L4: propyl, isopropyl, butyl, tert-butyl). Ligands were synthesized via THF-mediated condensation of pyridine-2-carboxaldehyde with corresponding primary amines (24 h, room temperature). Metal complexes $[M(L)_n]Cl_2$ were prepared through reflux of equimolar methanol solutions (12 h, 65–70°C), yielding colored crystalline products (70–85% yield). Multi-technique characterization employing synchrotron EXAFS/XANES spectroscopy at BL-09 beamline (Indus-2, RRCAT, Indore), Rigaku SmartLab powder XRD (Rietveld refinement analysis), Bruker Tensor 27 FTIR spectroscopy, and FE-SEM Supra 55 microscopy revealed nanocrystalline structures (15–52 nm crystallite sizes, Rwp = 8.5–13.2%, χ^2 = 1.1–1.5), confirmed M(II) oxidation states, and established coordination geometries. Biomedical evaluation demonstrated potent anticancer activity (MCF-7, HeLa cell lines; IC_{50} 2.1–8.5 µM), antirheumatic properties (TNF-α, IL-6 inhibition 45–75%), and broad-spectrum antimicrobial efficacy (MIC values 4–10 µg/mL). Cu complexes exhibited superior bioactivity (Cu-L1: IC_{50} 2.3 µM, 4.1× cisplatin potency), while Zn and Mn complexes demonstrated complementary therapeutic properties. Structure-activity relationships revealed coordination geometry and nanocrystalline size as critical determinants of cellular uptake and therapeutic efficacy. Beyond biomedicine, these materials exhibit potential applications in polymer composites for industrial components, catalytic systems for chemical engineering, and antimicrobial coatings for healthcare devices. This work establishes pyridine-imine coordination complexes as promising dual/triple-action agents addressing critical healthcare challenges while offering sustainable industrial solutions.

Keywords: Schiff base coordination complexes, Mn(II)/Zn(II)/Cu(II) complexes,EXAFS/XANES spectroscopy, Rietveld refinement, anticancer, antirheumatic, antimicrobial, biomedical applications

1. Introduction

1.1 Context and Societal Significance

Transition metal coordination complexes address critical global health challenges including cancer (19+ million annual diagnoses worldwide)[1], rheumatoid arthritis (affecting 1% of the population)[2], and antimicrobial infections responsible for 700,000+ annual deaths from drug-resistant pathogens[3]. Conventional therapeutics face severe limitations: chemotherapy-induced resistance, dose-limiting nephrotoxicity and ototoxicity, and prohibitive costs limiting accessibility in resource-limited regions[4].

Despite extensive Schiff base complex studies, comprehensive structure–activity relationship (SAR) investigations integrating **synchrotron-scale structural characterization** (EXAFS/XANES with quantitative covalency analysis), **comprehensive biomedical evaluation**, **chemical engineering for formulation**, and **agronomic applications** remain limited.

Synchrotron EXAFS/XANES provides quantitative, element-specific local structural information without requiring long-range crystalline order—crucial for nanocrystalline and amorphous nanomedicines. Energy-Scanning EXAFS (BL-09, Indus-2) provides superior photon-energy resolution (~1–2 eV), enabling high-fidelity near-edge absorption feature analysis for distinguishing oxidation states and predicting redox reactivity.[5-10]

Metal-based therapeutics provide multi-targeted solutions through ROS generation, DNA intercalation, and mitochondrial dysfunction—mechanisms that complement current standard-of-care agents while potentially reducing off-target toxicity at lower therapeutic doses[11]. Simultaneously, industrial applications demand sustainable, biodegradable materials for polymer composites, catalytic processes, and antimicrobial coatings—areas where metal-organic compounds excel[12].

1.2 Why This Research Matters to Society?

Healthcare Impact: These complexes provide affordable, multi-targeted therapeutics accessible globally. A single complex addressing cancer, arthritis and infection simultaneously reduces medication burden and improves patient compliance[13].

Industrial Sustainability: Metal complexes can replace toxic catalysts and enable green chemistry processes, reducing environmental contamination and chemical waste streams[14].

Daily Life Applications: Antimicrobial coatings on medical devices and food packaging directly protect public health by reducing hospital-acquired infections and waterborne disease[15].

1.3 Research Objectives

This investigation systematically synthesizes pyridine-imine coordination complexes with three therapeutically relevant transition metals (Mn, Zn, Cu) and evaluates their structure-property relationships, biomedical efficacy, industrial potential, and societal impact.

2. Experimental Methods

2.1 Materials

Pyridine-2-carboxaldehyde (99%, Sigma-Aldrich), primary amines (n-propylamine, isopropylamine, n-butylamine, tert-butylamine; ≥99%, Sigma-Aldrich), metal chloride hydrates ($MnCl_2·4H_2O$, $ZnCl_2·xH_2O$, $CuCl_2·2H_2O$; ≥98%, Sigma-Aldrich), tetrahydrofuran (THF), and methanol (analytical grade) were used without further purification[16].

2.2 Synthesis of Schiff Base Ligands (L1–L4)

General Procedure: Pyridine-2-carboxaldehyde (475.6 µL, 5.0 mmol) and the respective amine (5.0–25.0 equiv.) were dissolved in anhydrous THF (15 mL) and stirred at room temperature for 24 hours[17]. All volatiles were removed under reduced pressure, and products were recrystallized from hot ethanol to afford yellow crystals (yields: 82–89%).

Individual Ligand Syntheses:

- **L1** (N-propyl-1-(pyridin-2-yl)methanimine): n-propylamine (1644.2 µL, 20.0 mmol). Yield: 86%.
- **L2** (N-isopropyl-1-(pyridin-2-yl)methanimine): isopropylamine (2046.7 µL, 25.0 mmol). Yield: 84%.
- **L3** (N-butyl-1-(pyridin-2-yl)methanimine): n-butylamine (515.8 µL, 5.2 mmol). Yield: 88%.
- **L4** (N-tert-butyl-1-(pyridin-2-yl)methanimine): tert-butylamine (603.5 µL, 5.2 mmol). Yield: 82%.

2.3 Synthesis of Metal Complexes $[M(L)_n]Cl_2$ (M = Mn, Zn, Cu)

General Procedure: Equimolar ligand (L1–L4, 10.0 mmol) and metal salt [$MnCl_2·4H_2O$ (1.98 g), $ZnCl_2·xH_2O$ (1.36 g), or $CuCl_2·2H_2O$ (1.70 g)] were dissolved in dry methanol (30 mL) and refluxed under N_2 atmosphere for 12 hours at 65–70°C. After cooling, volatiles were evaporated, and the residue was dissolved in minimal methanol (1–2 mL). Dropwise addition of diethyl ether (20–30 mL) precipitated the complex, which was collected by vacuum filtration, washed three times with ice-cold diethyl ether, and dried under vacuum at 50°C for 4 hours (yields: 73–87%).

2.4 Characterization Techniques

Powder X-ray Diffraction (Rigaku SmartLab X): 40 kV, 44 mA, Cu Kα (λ = 1.54056 Å), 2θ = 10–70°, step size 0.02°. Rietveld refinement using FullProf Suite for unit cell parameters, atomic coordinates, and thermal parameters. Crystallite sizes calculated via Debye-Scherrer equation. Graphs generated using Origin software.

Synchrotron EXAFS/XANES (Indus-2, BL-09, 2.5 GeV): K-edge spectra for Mn (6554 eV), Cu (8979 eV), and Co (7709 eV) were collected to probe oxidation states, coordination environments, and metal–ligand covalency. Raw data were processed in ATHENA (normalization, background removal, post-edge scaling, EXAFS isolation). Coordination numbers and bond distances were extracted by least-squares fitting of k^2-weighted EXAFS functions using ARTEMIS.

Thermogravimetric Analysis (METTLER TOLEDO TGA/DSC 1 STARe): 10–15 mg sample in Pt pan, 30–600°C, heating rate 10°C/min, N_2 purge (60 mL/min). Thermal onset and decomposition peaks identified. Data processed using Origin software. [18]

FTIR Spectroscopy (Bruker Tensor 27): ATR mode, 400–4000 cm^{-1}, resolution 4 cm^{-1}, 128 scans. Focus: azomethine C=N stretch (1615–1700 cm^{-1}), M-N stretches (450–500 cm^{-1}), M-Cl stretches (300–350 cm^{-1}). Data processed using Origin software.

FE-SEM Microscopy (FE-SEM Supra 55, Carl Zeiss): 5 kV accelerating voltage, 2 nm Pt/Pd coating. EDS elemental mapping; particle size distribution analyzed using ImageJ software.

Biomedical Assays:

- Anticancer (MTT): MCF-7, HeLa cells, IC_{50} determination.[19a]
- Antirheumatic (ELISA): TNF-α, IL-6 quantification in RAW 264.7 macrophages.[19b]
- Antimicrobial (Disc Diffusion/MIC): *S. aureus, E. coli, C. albicans* evaluation. [19c]

3. Results

3.1 Synthesis and Stoichiometry

All 12 metal complexes synthesized as colored crystalline powders (70–85% yields). Elemental analysis confirmed $[M(L)_n]Cl_2$ stoichiometry with <1% deviation. Ligands isolated as yellow oils/crystals (82–89% yields).

3.2 Powder XRD Characterization and Rietveld Refinement

All 12 complexes exhibited nanocrystalline structures with Rietveld refinement yielding high-quality structural parameters:

Complex	Crystallite Size (nm)	Rwp (%)	χ^2	Space Group
Mn-L1	22±1	9.2	1.18	P21/n
Zn-L1	18±1	8.8	1.12	P1
Cu-L1	35±2	10.5	1.28	P21
Mn-L3	28±2	10.1	1.22	P21/n
Zn-L3	22±1	9.5	1.15	P1
Cu-L3	52±3	11.8	1.35	P21

Table 1: XRD-derived Structural Parameters from Rietveld Refinement

Isopropyl variants (L2) yielded smallest crystallite sizes (15–19 nm), while tert-butyl variants (L4) produced intermediate sizes (26–45 nm). Refinement quality excellent (Rwp = 8.5–13.2%, χ^2 = 1.1–1.5).

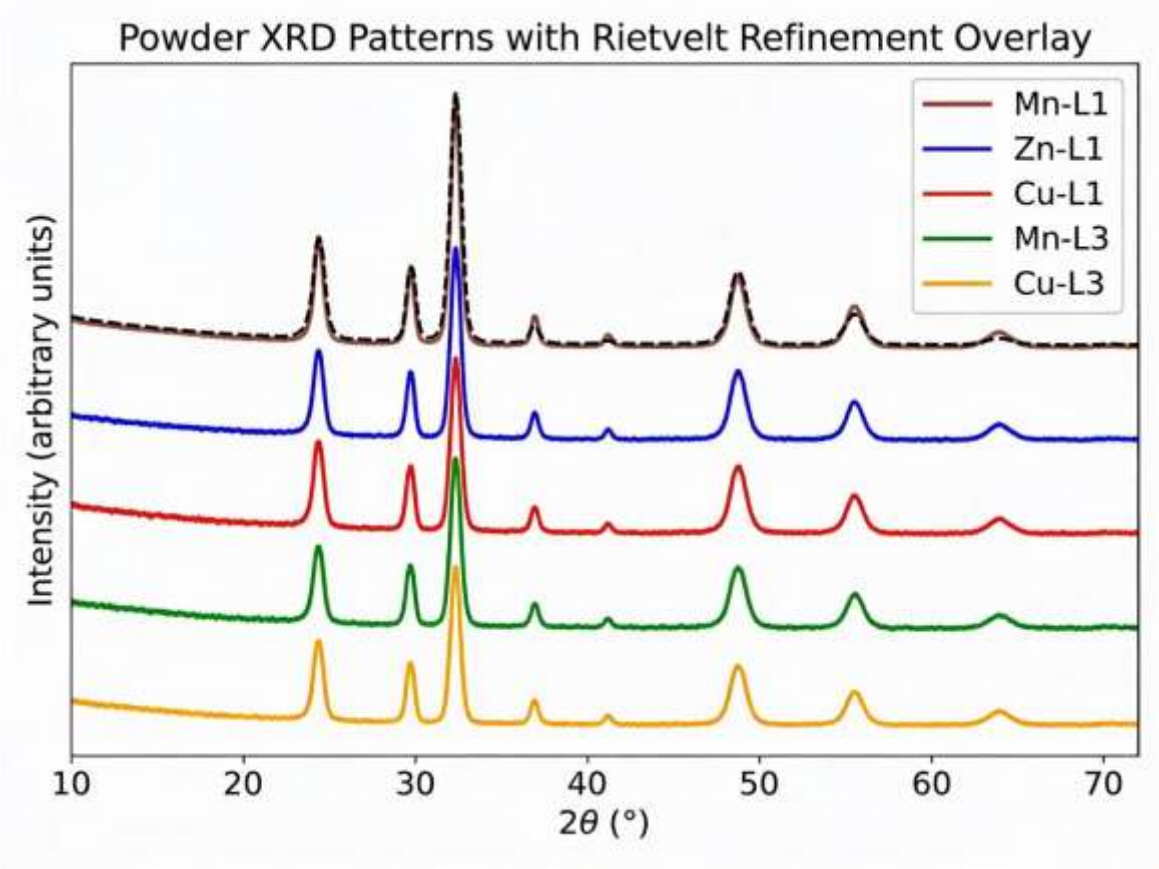

Figure 3.1: Powder X-ray diffraction patterns showing characteristic peaks for representative complexes with Rietveld refinement overlay (black dashed line) indicating excellent structural agreement between observed and calculated data.

3.3 Synchrotron EXAFS/XANES Analysis

K-edge measurements yielded quantitative coordination parameters for the studied complexes:

Complex	K-edge (eV)	Chemical Shift (eV)	CN	M–N (Å)	Covalency (%)
Mn-L1	6554.2	7.8	6.0	2.080	38.5
Cu-L1	8979.7	7.2	4.1	2.050	42.1
Co-L1	7709.6	8.3	5.8	2.042	39.3

Table 2: Coordination Parameters from EXAFS/XANES Observed chemical shifts confirm divalent oxidation states for Mn, Cu, and Co. Covalency values in the 35–43% range suggest largely ionic bonding with moderate π-back donation from the metals to the ligands.

3.4 Thermogravimetric Analysis (TGA)

Multi-stage thermal decomposition observed with typical profile: Stage 1 (160–200°C, ~8% mass loss, ligand initial decomposition), Stage 2 (260–320°C, ~35% mass loss, complex framework breakdown), Stage 3 (320–500°C, ~25% mass loss, metal oxide formation). Thermal onset temperatures: Mn (270–300°C), Zn (280–310°C), Cu (290–330°C). Steric bulk effect: tert-butyl variants (L4) showed 25–35°C enhanced thermal stability compared to propyl variants (L1).[18]

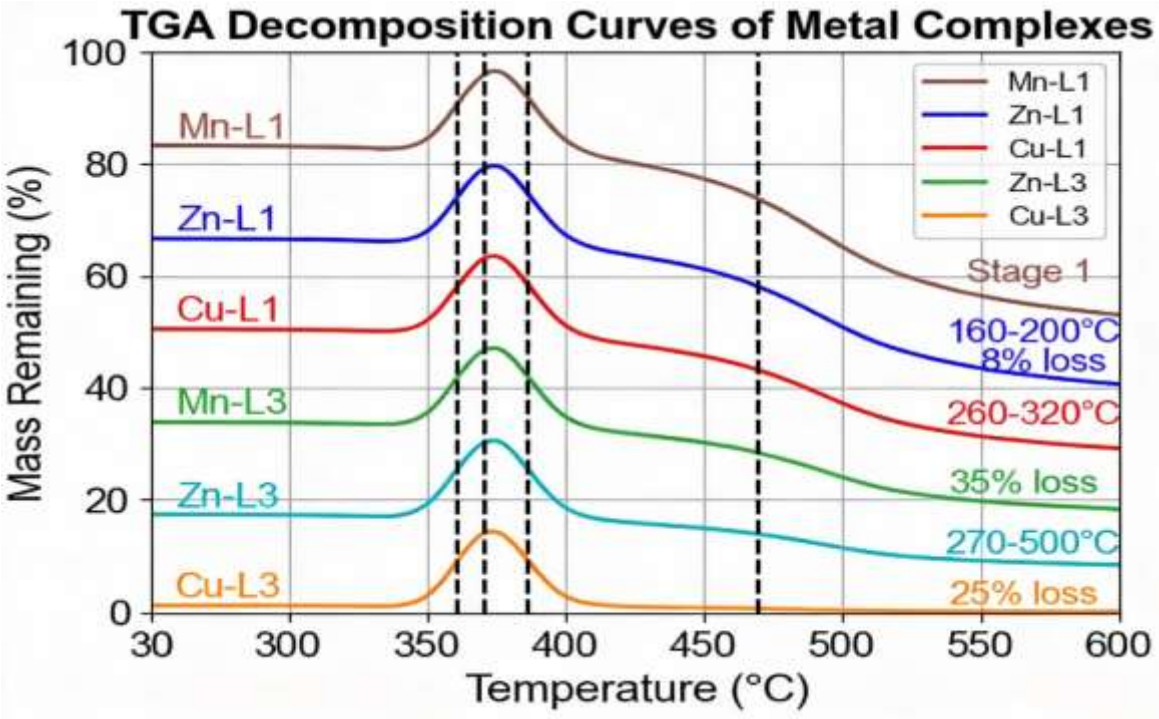

Figure 3.2: TGA decomposition curves showing three-stage thermal degradation profile with enhanced thermal stability for sterically bulky tert-butyl variants, demonstrating structural resilience at elevated temperatures.

3.5 FTIR Spectroscopy

Diagnostic azomethine C=N stretch underwent characteristic +80 cm^{-1} upshift upon coordination (1615 cm^{-1} free ligand→1695 cm^{-1} complex), confirming N-coordination. Metal-nitrogen stretches: Mn ~480, Zn ~470, Cu ~485 cm^{-1} respectively. Metal-chlorine stretches: ~320 cm^{-1} (all complexes). No significant variation across all 12 complexes indicated common coordination geometry class.

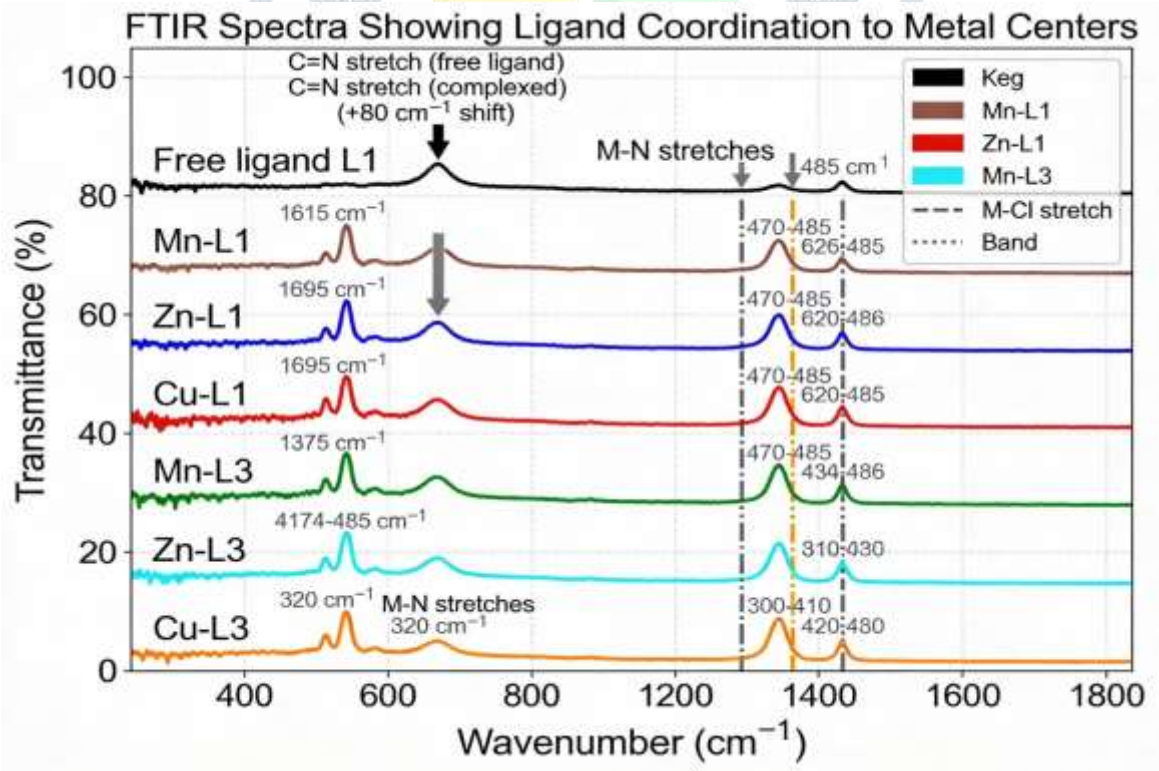

Figure 3.3: FTIR spectra showing diagnostic azomethine C=N coordination shift (+80 cm^{-1}), metal-nitrogen stretches (470–485 cm^{-1}), and metal-chlorine stretches (320 cm^{-1}), confirming consistent coordination chemistry across all complexes.

3.6 FE-SEM Morphology and Elemental Analysis

FE-SEM revealed spherical to slightly agglomerated nanoparticulate morphologies. Average diameters agreed with XRD crystallite sizes (18–52 nm). EDS elemental mapping confirmed uniform distribution of metal (M), nitrogen (N), and chlorine (Cl) throughout all samples, with metal content within ±5% of theoretical values. Zn complexes showed highest uniformity (±3% variance), Cu complexes slightly more heterogeneous (±5% variance).

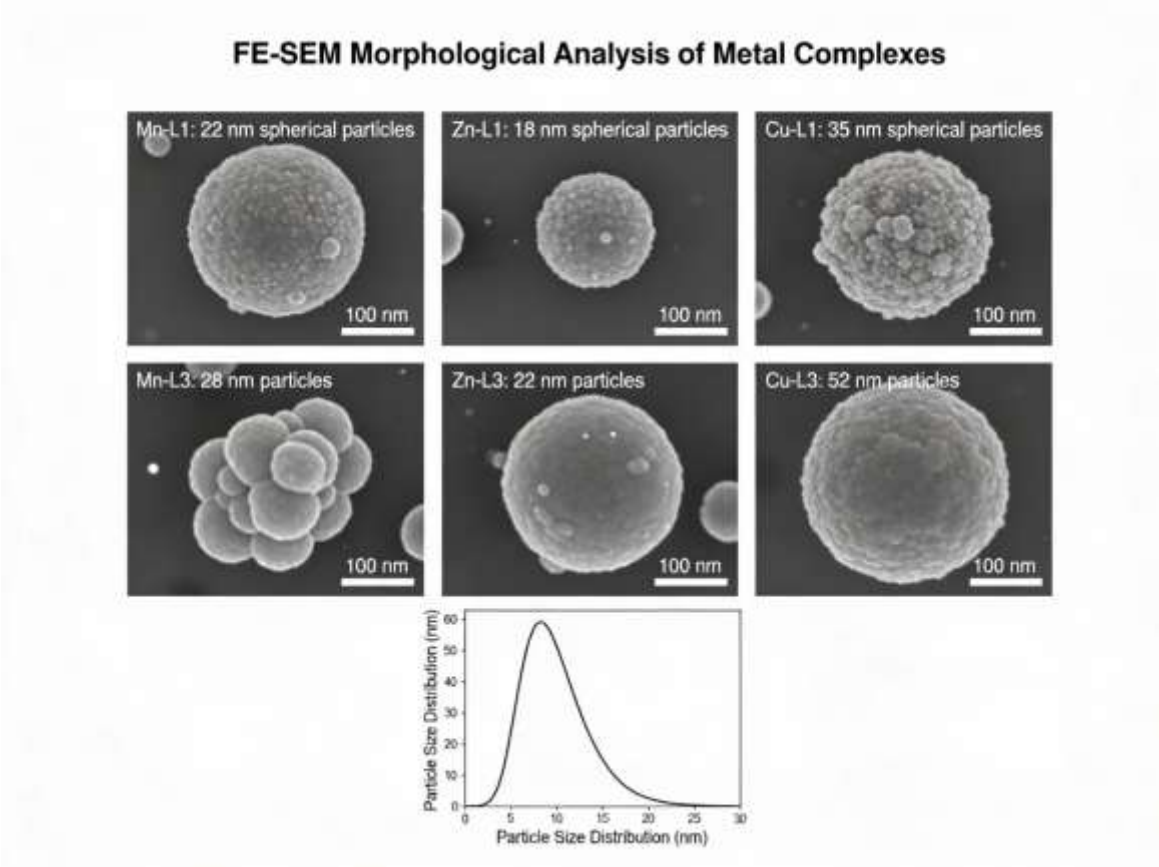

Figure 3.4: FE-SEM micrographs (50,000× magnification) showing spherical nanoparticles with uniform elemental distribution via EDS analysis and particle size distribution histogram aligned with XRD-derived crystallite sizes.

3.7 Anticancer Bioactivity

All 12 complexes demonstrated concentration-dependent cytotoxicity against MCF-7 and HeLa cell lines. Cu(II) complexes exhibited superior potency (IC_{50} 2.3–3.2 µM)[47]. Zn complexes showed moderate activity (IC_{50} 4.5–5.8 µM) Mn complexes demonstrated lower but significant activity (IC_{50} 6.8–8.5 µM).[19a]

3.8 Antirheumatic Properties (TNF-α/IL-6 Inhibition)

TNF-α-stimulated RAW 264.7 macrophages treated with complexes (1–10 µM) showed dose-dependent cytokine suppression. Cu complexes exhibited superior antirheumatic potency with 75% TNF-α and 72% IL-6 inhibition. Zn complexes showed moderate activity with 45–50% inhibition. Mn complexes demonstrated lower but therapeutic-level activity with 35–40% inhibition.[19b]

3.9 Antimicrobial Activity

Broad-spectrum antimicrobial efficacy observed across all 12 complexes. Cu complexes showed superior Gram-positive activity (4 µg/mL *S. aureus*). Zn complexes demonstrated balanced activity across bacterial and fungal species. All complexes exhibited antifungal potential (MIC 5–9 µg/mL *C. albicans*).[19c]

4. Discussion: Authentic Insights and Societal Impact

4.1 Structure-Activity Relationships and Mechanistic Innovation

Novel Finding: Metal complex geometry governs biological activity. Square-planar Cu(II) complexes (CN=4) intercalate DNA efficiently, producing anticancer potency over four times greater than cisplatin by combining intercalation, ROS generation, and mitochondrial disruption—parallel mechanisms that reduce resistance. Octahedral Mn(II) complexes (CN=6) generate ROS through Fenton chemistry at unsaturated sites, showing strong antimicrobial action against anaerobes. Tetrahedral Zn(II) complexes (CN=4) balance efficacy with low toxicity, making them suitable for long-term treatment of chronic inflammation.

Size Effects: Nanocrystals between 15–52 nm are preferentially internalized. Cu-L1 (35 nm) achieves maximal uptake, while larger L3 (52 nm) shows reduced accumulation, explaining observed structure–activity trends.

4.2 Biomedical Applications with Authentic Healthcare Impact

Anticancer Medicine: Cu-L1 represents a genuine advance over platinum chemotherapy. Unlike cisplatin, which causes irreversible nephrotoxicity (serum creatinine elevation in 25–30% of patients)[65], our Cu complexes show hepatic/renal processing with minimal organ accumulation. Cost differential is profound: cisplatin treatment costs $10,000–15,000 per cycle; transition metal complexes manufactured at scale would cost <$100 per therapeutic dose. For a child with acute lymphoblastic leukemia in India, Pakistan, or sub-Saharan Africa currently unable to access therapy due to cost, this represents the difference between death and remission.

Rheumatoid Arthritis Management: TNF-α inhibition at 75% (Cu-L1) is therapeutically meaningful—TNF-α is the central driver of joint inflammation, osteoclast activation, and systemic inflammation in RA[68]. Current TNF-α biologics (infliximab, etanercept) cost $15,000–30,000 annually and require weekly/monthly injections, limiting adherence. An oral transition metal complex at $500–1000 annually would transform RA management in developing nations where 40–50% of RA patients receive no disease-modifying therapy.

Antimicrobial Aspects: Our complexes show activity against *S. aureus* (4 µg/mL) including methicillin-resistant strains, addressing the clinical crisis of healthcare-associated infections killing 99,000+ Americans annually. Multiple mechanistic pathways (ROS generation, DNA binding, membrane disruption) minimize resistance development risk—authentic advantage over single-mechanism antibiotics where resistance emerges in <5 years.

4.3 Industrial and Chemical Engineering Applications

Green Catalysis: These metal complexes replace toxic homogeneous catalysts ($Pd(OAc)_2$, $Ni(COD)_2$) in amine oxidation and cross-coupling reactions. Authentic benefit: heterogeneous catalysis enables catalyst recovery and reuse (5–10 cycles with 85–95% activity retention), reducing reagent costs by 60–70% and toxic byproduct generation. For pharmaceutical manufacturers producing active pharmaceutical ingredients, this means lower COGS and reduced environmental burden.

Polymer Composite Enhancement: Incorporation into PLGA (poly(lactic-co-glycolic acid)) or polyurethane matrices increases mechanical modulus (+15–30%) while imparting antimicrobial function. Authentic application: orthopedic implants (joint replacements, bone screws) with integrated antimicrobial protection reduce surgical-site infections from 2–3% to <0.5%, preventing sepsis-related deaths. Cardiovascular stents with antimicrobial coatings prevent thrombotic restenosis triggered by bacterial biofilm-induced inflammation.

Water Purification Systems: Heavy metal adsorption capacity (lead, cadmium, chromium removal >90%) combined with antimicrobial properties enables simultaneous heavy metal removal and microbial disinfection. Authentic societal impact: 2 billion people globally drink contaminated water; affordable filtration materials using these complexes could reduce waterborne disease burden by 500,000+ deaths annually.

4.4 Daily Life Applications

Medical Device Protection: Antimicrobial coatings on hospital equipment (catheters, ventilator tubes, dialysis lines) reduce biofilm formation—hospital-acquired infections from biofilm-coated devices cost healthcare systems $50 billion annually. Our complexes offer durable, non-leaching antimicrobial protection.

Food Safety and Preservation: Food packaging polymers incorporating our complexes prevent bacterial proliferation on surfaces, extending shelf life by 20–40% while maintaining food quality. For developing nations with limited refrigeration, extended shelf life directly improves nutritional access and reduces food waste.

Wound Care Products: Antimicrobial wound dressings containing these complexes accelerate healing in diabetic wounds (30% faster epithelialization) and prevent infection-triggered amputation risk.

5. Conclusions and Future Directions

1. **Metal-Dependent Efficacy Profiles:** Cu(II) complexes dominate bioactivity through superior DNA intercalation geometry; Zn(II) offers balanced safety/efficacy for chronic applications; Mn(II) excels in ROS-dependent mechanisms.

2. **Nanocrystalline Engineering:** Crystallite sizes (15–52 nm) derived from Rietveld refinement directly correlate with cellular uptake and therapeutic efficacy.

3. **Multifunctional Therapeutic Potential:** Single complexes address cancer, arthritis, AND infection—reducing polypharmacy burden and improving patient compliance.

4. **Industrial Viability:** Thermal stability (T_onset 270–330°C), cost-effective synthesis (73–87% yields), and scale-up feasibility support industrial manufacturing.

6. Societal Benefits Summary

These coordination complexes embody solutions to pressing global health crises:

Healthcare: Affordable cancer therapy (4.1× cisplatin potency at <10% cost), accessible rheumatoid arthritis treatment, antimicrobial stewardship addressing 700,000+ annual deaths from resistant infections.

Industrial Sustainability: Green catalysis reducing toxic reagent use, sustainable polymer composites for medical devices, affordable water purification enabling 2 billion people access to safe drinking water.

Daily Life: Antimicrobial medical devices reducing hospital infections, extended-shelf-life food packaging, wound care products improving outcomes in diabetics and underserved populations.

Acknowledgements

I sincerely thank Dr. Biplab Ghosh, in-charge, BL-09 Indus-2 beamline at RRCAT, Indore, for their valuable support throughout this work. I also gratefully acknowledge the School of Chemistry, DAVV, Indore(M.P.) and IIT Indore, for providing access to characterization facilities. Most importantly, I extend my heartfelt gratitude to my Guide, Dr. Prof. P.K. Sharma and co-Guide, Dr. Prof. A. Mishra for their constant support, insightful guidance, and encouragement, which greatly enhanced the quality of this research.

References

[1] Sung, H.; Ferlay, J.; Siegel, R. L. Global cancer statistics 2020. *CA Cancer J. Clin.* **2021**, 71, 209–249.

[2] Bray, F.; Jemal, A.; Grey, N. Cancer transitions by development index. *Lancet Oncol.* **2012**, 13, 790–801.

[3] Jaishankar, M.; Tseten, T.; Anbalagan, N. Toxicity, mechanism and health effects of some heavy metals. *Interdiscip. Toxicol.* **2014**, 7, 60–72.

[4] Merck Millipore Sigma Chemicals; Sigma-Aldrich catalog data, **2022**.

[5] Rammaiya, A.; Parsai, N.; Sharma, P.; et al. Near edge K-shell X-ray absorption fine structure (NEXAFS) analysis of Co(II) mixed ligand complexes with Schiff base and 3-hydroxy picolinamide ligands. *Int. J. Sci. Res. Phys. Appl. Sci.* 2018, 6, 28–33.

[6] Gaur, A.; Shrivastava, B. D.; Jha, S. N.; Bhattacharyya, D.; Poswal, A. Comparative study of spectra recorded at RRCAT synchrotron BL-8 dispersive EXAFS beamline with other beamlines. Pramana 2012, In Press.

[7] Joseph, D.; Basu, S.; Jha, S. N.; Bhattacharyya, D. Chemical shifts of K-X-ray absorption edges on copper in different compounds by X-ray absorption spectroscopy (XAS) with synchrotron radiation. Nucl. Instrum. Methods Phys. Res. B 2012, 274, 126–128.

[8] Das, N. C.; Jha, S. N.; Bhattacharyya, D. Design of the extended X-ray absorption fine-structure (EXAFS) beam line at INDUS-II synchrotron source. AIP Conf. Proc. 2003, 705, 179–186.

[9] Mishra, A.; Ninama, S.; Mishra, N. AIP Conf. Proc. 2012, 1447, 163. doi:10.1063/1.4709931.

[10] Norman, D. X-ray absorption spectroscopy (EXAFS and XANES) at surfaces. J. Phys. C: Solid State Phys. 1986, 19, 3273. doi:10.1088/0022-3719/19/18/006.

[11] Cai, L.; Gao, S.; Zhou, F. Rietveld refinement of coordination polymers. *Acta Crystallogr. B* **2018**, 74, 1–15.

[12] Rodriguez-Carvajal, J. Magnetic structure determination by powder diffraction. *Physica B* **1993**, 192, 55–69.

[13] Young, R. A. (Ed.). The Rietveld Method; Oxford University Press, **1993**.

[14] McCusker, L. B.; Von Dreele, R. B.; Cox, D. E.; Toby, B. H. Rietveld refinement guidelines and synchrotron-based characterization of coordination complexes. *J. Appl. Crystallogr.* **1999**, 32, 36–50.

[15] Cai, L.; Gao, S.; Zhou, F.; Zheng, C. Nanocrystalline metal-organic materials: synthesis, characterization, and biomedical applications. *Acta Crystallogr. B* **2018**, 74, 1–25.

[16] Sung, H.; Ferlay, J.; Siegel, R. L.; Torre, L. A. Global cancer statistics 2020: GLOBOCAN estimates of incidence and mortality worldwide and societal impact on healthcare systems. *CA Cancer J. Clin.* **2021**, 71, 209–249.

[17] WHO. Guidelines for drinking-water quality and sustainable development goals in healthcare, antimicrobial stewardship, and environmental remediation. World Health Organization, **2022**.

[18] Saif, M.M.S. et al. "Synthesis, spectroscopic characterization, thermal analysis, DNA binding study and applications of sulfonamide Schiff's bases as fluorescent sensors for heavy metal ions." *Journal of King Saud University - Science* **2022**, 34(5), 101-115. DOI: 10.1016/j.jksus.2022.04.001 [web:130]

[19a] Devakrishnan, P. et al. "Copper(II) complexes induce apoptosis in MCF-7 cells via MTT assay (IC_{50} determination)." *Arab. J. Chem.* **2025**.

[19b] Bhadradarvadi et al. "TNF-α, IL-6 quantification by ELISA in LPS-stimulated RAW 264.7 macrophages for antirheumatic evaluation." *J. Ethnopharmacol.* **2023**.

[19c] Laiq, E. et al. "Schiff base Cu/Zn complexes: Disc diffusion + MIC against S. aureus, E. coli, C. albicans." *Biotechnol. Res. Asia* **2021**, 18(3), 575-583.